

RESEARCH

Open Access



Zebrafish and cellular models of *SELENON*-Congenital myopathy exhibit novel embryonic and metabolic phenotypes

Pamela Barraza-Flores¹, Behzad Moghadaszadeh¹, Won Lee¹, Biju Isaac², Liang Sun², Emily T. Hickey¹, Shira Rockowitz^{1,2}, Piotr Sliz^{2,3} and Alan H. Beggs^{1*} 

Abstract

Background *SELENON*-Congenital Myopathy (*SELENON*-CM) is a rare congenital myopathy caused by mutations of the *SELENON* gene characterized by axial muscle weakness and progressive respiratory insufficiency. Muscle histopathology may be non-specific, but commonly includes multiminicores or a dystrophic pattern. The *SELENON* gene encodes selenoprotein N (SelN), a selenocysteine-containing redox enzyme located in the endo/sarcoplasmic reticulum membrane where it colocalizes with mitochondria-associated membranes. However, the molecular mechanism(s) by which SelN deficiency cause *SELENON*-CM remain poorly understood. A hurdle is the lack of cellular and animal models that show easily assayable phenotypes.

Methods Using CRISPR-Cas9 we generated three zebrafish models of *SELENON*-CM, which were then studied by spontaneous coiling, hatching, and activity assays. We also performed *selenon* coexpression analysis using a single cell RNAseq zebrafish embryo-atlas. SelN-deficient myoblasts were generated and assayed for glutathione, reactive oxygen species, carbonylation, and nitrosylation levels. Finally, we tested *Selenon*-deficient myoblasts' metabolism using a Seahorse cell respirometer.

Results We report deep-phenotyping of SelN-deficient zebrafish and muscle cells. SelN-deficient zebrafish exhibit changes in embryonic muscle function and swimming activity in larvae. Analysis of single cell RNAseq data in a zebrafish embryo-atlas revealed coexpression of *selenon* and genes involved in the glutathione redox pathway. SelN-deficient zebrafish and mouse myoblasts exhibit altered glutathione and redox homeostasis, as well as abnormal patterns of energy metabolism, suggesting roles for SelN in these functions.

Conclusions These data demonstrate a role for SelN in zebrafish early development and myoblast metabolism and provide a basis for cellular and animal model assays for *SELENON*-CM.

Keywords Selenoprotein N, Multimini-core myopathy, Rigid spine muscular dystrophy, Congenital myopathy, Zebrafish model

*Correspondence:

Alan H. Beggs
beggs@enders.tch.harvard.edu

¹Division of Genetics and Genomics, The Manton Center for Orphan Disease Research, Boston Children's Hospital, Harvard Medical School, Boston, MA, USA

²Research Computing, Information Technology Department, Boston Children's Hospital, Boston, MA, USA

³Division of Molecular Medicine, The Manton Center for Orphan Disease Research, Boston Children's Hospital, Harvard Medical School, Boston, MA, USA



© The Author(s) 2025. **Open Access** This article is licensed under a Creative Commons Attribution-NonCommercial-NoDerivatives 4.0 International License, which permits any non-commercial use, sharing, distribution and reproduction in any medium or format, as long as you give appropriate credit to the original author(s) and the source, provide a link to the Creative Commons licence, and indicate if you modified the licensed material. You do not have permission under this licence to share adapted material derived from this article or parts of it. The images or other third party material in this article are included in the article's Creative Commons licence, unless indicated otherwise in a credit line to the material. If material is not included in the article's Creative Commons licence and your intended use is not permitted by statutory regulation or exceeds the permitted use, you will need to obtain permission directly from the copyright holder. To view a copy of this licence, visit <http://creativecommons.org/licenses/by-nc-nd/4.0/>.

Background

SELENON-Congenital Myopathy (*SELENON*-CM) is a rare congenital myopathy caused by mutations of the *SELENON* gene [1, 2]. It has an estimated incidence of 1 in 200,000 births [3, 4]. However, based on population estimates of carrier frequencies the incidence may be significantly higher when considering undiagnosed cases. *SELENON*-CM has a clinical onset mostly before two years of age but may also present as late as early to mid-adulthood [5, 6]. It is typically congenital in onset, as evidenced by a high arched palate in almost two-thirds of children, neonatal hypotonia in as many as one-third, and occasional equinovarus foot. Childhood is characterized by development of early-onset spinal rigidity, axial muscle weakness, scoliosis, and respiratory insufficiency requiring nocturnal ventilation; however, the great majority of patients remain ambulant throughout their lives. There is currently no cure or specific treatment for *SELENON*-CM. Patients' muscle biopsies show heterogeneous histopathological changes that have led to the classification of this disease as rigid spine muscular dystrophy (RSMD) [1], multimincore disease [2], congenital fiber type disproportion [7], and Desmin-related myopathy with Mallory-like body inclusions [8, 9]. However, these changes are not specific and are not universally found in patients. The most common histopathological findings are multimincore lesions, which reflect areas of mitochondrial loss [10]. Additionally, natural history studies in *SELENON*-CM patients report metabolic abnormalities, including insulin-resistance [11] as well as altered body mass index, both of which correlate with disease severity [12, 13].

The *SELENON* gene encodes selenoprotein N (SelN), which is a member of the selenoprotein family [14]. Selenoproteins are a group of selenocysteine-containing proteins involved primarily in oxidoreduction reactions. Selenocysteine residues in these proteins are typically involved in enhancing redox catalytic activity [15]. SelN is an endo/sarcoplasmic reticulum (ER/SR)-resident glycoprotein with a transmembrane domain [16], thiol reductase catalytic activity, and a calcium binding EF-hand domain [17]. SelN has been proposed as an important ER/SR redox protein that plays an essential role in cell protection against oxidative stress and modulation of SERCA channel activity [18–20]. Previous studies suggest that inducing ER stress in SelN-deficient myoblasts can contribute to increased pathological phenotypes [11, 18]. SERCA channels are redox partners of SelN, and lack of SelN leads to SERCA channel hyper-oxidation and inactivation, resulting in reduced calcium uptake to the ER/SR. While this mechanism likely contributes to delayed myofiber relaxation [18], it is probably not the only pathophysiological mechanism leading to weakness in *SELENON*-CM patients. SelN also colocalizes

with Mitochondria Associated Membranes (MAMs) that tether the mitochondria to the ER [12]. MAMs allow for Ca^{2+} influx from the ER into the mitochondria, phospholipid synthesis and transport, regulation of mitochondrial dynamics, among other vital cell functions [21, 22]. Based on these findings, we hypothesize that mitochondria dysregulation may play a vital role in the pathogenesis of *SELENON*-CM.

SELENON is expressed broadly in mature tissues throughout the body, but its highest levels of expression are during early developmental stages [16]. In situ hybridization studies have shown that *Selenon* transcripts in mouse and zebrafish embryos are located in developing notochord and somite regions [16, 23–26], suggesting an important role during early muscle development. Even though there is an identified pattern of expression during embryogenesis and some known molecular functions of SelN, one of the main obstacles for the study of *SELENON*-CM has been an inability to demonstrate a robust disease phenotype in animal and cellular models. Previously, our group developed a *Selenon* null mouse model for the study of this disease [27]. We found changes in lung development and mild core lesions in the muscle could be observed only when the mice were subjected to oxidative stress via vitamin E deficiency and forced endurance running. Other groups have shown a fatigue-induced phenotype in ex vivo mechanical studies of a similar *Selenon* null mouse model [28], however, clinical signs of myopathy were not readily apparent. Although cellular models of *SELENON*-CM have been used to describe molecular mechanisms of SelN [12, 17, 18, 20], robust functional assays that might become the basis for drug development have been difficult to develop. Several morpholino-based transient models of SelN knock-down in zebrafish have been reported [26, 29], but it is unclear what aspects of the phenotypes were due to SelN deficiency and what might be off-target consequences of the morpholinos. No stable zebrafish models of germline *selenon* knock-out have been reported to date. In this project, we aim to deep-phenotype new zebrafish and cellular knock-out models for the study of *SELENON*-CM while elucidating SelN functional roles in muscle metabolism.

Methods

Statistical analysis

Statistical calculations were performed using GraphPad Prism 10 software. Student's *t* test was used to compare means between two groups of data and one-way ANOVA was used to compare three or more groups of data. ANOVA calculations were followed up by Tukey's multiple comparison test to determine differences between samples. Means of experimental groups were considered significant when *p* value was <0.05.

Generation of *SELENON-CM* zebrafish models

To generate zebrafish lines with mutations in the *selenon* gene, we induced mutagenesis using CRISPR-Cas9 system Gene Art Platinum Cas9 Nuclease (Thermo Fisher Scientific, Waltham, MA). This was achieved by performing mRNA microinjections into one-cell AB zebrafish embryos targeting exon 2. The guide RNA (gRNA) used to target this exon was 5'-AUU GUA GGA GGC AGG ACU GA-3'. This resulted in the generation of mosaic mutations in exon 2 of the *selenon* gene. These eggs were then reared and bred to AB wild type (WT) fish to generate heterozygous carriers. After Sanger sequencing and selecting mutations of interest fish were outbred to AB WT. Finally, each heterozygous mutation was intercrossed to generate experimental fish: homozygous knock outs (KO), heterozygotes (HET), and WT in ratios of 1:2:1.

Zebrafish real time qPCR

We quantified *selenon* transcripts in zebrafish using PrimePCR multiplex real time quantitative PCR (RT-qPCR) system by Bio-Rad (Hercules, CA). We extracted and purified total RNA from cells and zebrafish using Trizol LS reagent (Ambion) following protocol by Peterson et al., 2009 [30]. Reverse transcription and qPCR assays were performed using Reliance One-step multiplex RT-qPCR Master Mix (Bio-Rad). We included two housekeeping genes determined by Reference Gene H384 panel by Bio-Rad: *rps18* and *ppia*. Analysis was performed using CFX Maestro Software by Bio-Rad.

Zebrafish western blotting

For protein quantification of SelN in zebrafish embryos, we created new antibodies against the C-terminal domain of SelN for both zebrafish and mouse isoforms (Biomatik, Kitchener, Ontario). The amino acid sequence targeted for these antibodies were QEGLEKAKPYLES for zebrafish and KEGLRRGLPLLQP for mouse. Cells and 2 days post fertilization (dpf) de-yolked and dechorionated zebrafish (according to [31]) were extracted for total protein using RIPA lysis buffer (Thermo Fisher Scientific) with protease inhibitors (Thermo Fisher Scientific). Using NuPAGE-Tris Acetate western blot system by Invitrogen (Carlsbad, CA) we separated our proteins by size and transferred them onto a PDVF blot. Ponceau stain (Sigma Aldrich, St Louis, MO) was used to image total protein transferred. Finally, we immunoblotted against SelN at a 1:500 dilution and rhodamine labeled anti-tubulin antibody (Bio-Rad) at 1:5,000 concentration. Blots were imaged using a ChemiDoc MP Imaging System by Bio-Rad.

Zebrafish spontaneous coiling assay

To measure spontaneous coiling, we set up zebrafish breeding pairs overnight with dividers and began mating the following day. Fish were harvested in windows of 30 min and time was annotated to maintain consistency. Twenty-four hours later, embryos were placed under a light microscope and recorded for 3 min. Cycles of ~15 embryos were recorded alternating mutant and WT fish for one hour. To quickly fit ~15 embryos under the microscope field of view we 3D printed a 1.4 mm wide grid (Supplemental File 1). Videos were analyzed using DanioScope version 1.1 software (Noldus, Wageningen, the Netherlands).

Zebrafish hatching assay

To measure changes in hatching we set up HET by HET zebrafish breeding pairs overnight with dividers and began mating them the following day at the same time. One hour later we harvested the eggs and allowed them to grow overnight. On day 1 post-fertilization eggs were transferred to three 96-well plates for observation. Hatching counts were performed 4 times a day until all eggs had hatched. On 4 dpf fish were euthanized and genotyped.

Zebrafish swim activity assay

Six dpf zebrafish larvae were placed in 48-well plates and tested for swim activity using an activity monitor by Zantiks (Cambridge, UK). The protocol used during activity recording included: 10 min acclimation, 20 s vibration, 5 min light, 5 min dark, 5 min light, 5 min dark, and then repeat the same steps. Data were analyzed using an in-house generated MatLab script (see Supplemental File 2).

Analysis of embryonic zebrafish single cell RNAseq atlas

Single-cell RNAseq (scRNAseq) data from Wagner et al. 2017 [24] were downloaded. We extracted gene expression data using the Python package scanpy v1.9.1. In total, 30,677 genes with their averaged expression data across six samples in the scRNAseq data were extracted. 903 genes were removed during QC step for having missing data and/or zero variance. Expression matrix was loaded on R version 4.0.2 for analysis. Adjacency matrix for the remaining 29,774 genes was generated using the Weighted Gene Correlation Network Analysis (WGCNA) package [32]. Soft thresholding from the scale-free topology model was used to reduce 'noise' of correlations in the adjacency matrix. A Topology Overlap Matrix (TOM) was generated from the adjacency matrix and converted to a dissimilarity matrix by subtracting the TOM matrix from 1. Samples were clustered using the 'hclust average' method. 136 gene modules were identified using the dynamic tree cut method on the generated clusters using the WGCNA R package with a minimum

of 30 genes per module. To distinguish between these, modules were labeled as colors using the labels2colors function. Twenty core merged modules were generated by merging modules with a similar matrix (distance threshold < 0.25). The genes in each module demonstrate a similar expression profile and co-express. Pearson correlation was generated for each module against clinical traits, i.e., time point. Significance of the correlation of each gene against the time point was computed. Two core modules, 'antiquewhite1' (4516 genes) and 'firebrick2' (240 genes) having significant p-values < 0.05 for correlation with *selenon* were identified. 3339 genes with positive association (weighted threshold > 0.02) to *selenon* (*sepn1*) from 'antiquewhite1' and 168 genes from 'firebrick2' modules were exported using the exportNetworkToCytoscape function and were used to generate interaction networks on Cytoscape v3.8.2 software. KEGG pathway and GO term enrichment analysis of significant modules was performed using clusterProfiler package (v3.16.0) [33]. Enriched pathways were identified as terms with $p_{adj} < 0.05$.

Cell culture

C2C12 mouse myoblasts (American Type Culture Collection, Manassas, VA) were maintained in growth medium (DMEM supplemented with 20% Fetal Bovine Serum, Certified; GIBCO, (Invitrogen) in 10% CO₂. For differentiation, cells were allowed to grow to 90–100% confluence and switched to differentiating medium (DMEM containing 2% Horse Serum; GIBCO, Invitrogen) that was subsequently changed every 24 h.

C2C12 *selenon* knock down

RNAi-Ready pSIREN-RetroQ vector (Clontech, Inc. Mountain View, CA) was used to prepare shRNA constructs targeting *Selenon* gene (KD1: TTCAAACCCAT TGCGGAGA, KD2: GCAAACCATGAATTGGAAAGT, and KD3: CATGATTGACAGCCGCCTG). These constructs were transfected into the 293 Ecopack packaging cell line (Clontech) using Lipofection 2000 transfection reagent (Invitrogen) to generate retrovirus particles. 48 h after transfection, the viral supernatant was harvested and used for transduction of C2C12 cells. The virus was removed 6 h after the infection and fresh growth medium containing puromycin was added to C2C12 cells allowing the selection of infected cells. For each shRNA target 3 replicate plates of C2C12 cells were transduced and were subsequently processed as independent cultures.

Cellular RNA extraction and qRT-PCR

Total RNA was extracted and purified from C2C12 cells using RNeasy kit (Qiagen, Valencia, CA) according to the manufacturer's instructions. RNA was treated with DNase I Amplification Grade (Invitrogen). cDNA

synthesis preparation was performed using the SuperScript First-Strand synthesis system for RT-PCR (Invitrogen). Real-time quantitative RT-PCR was carried out using the TaqMan probe-based chemistry (Applied Biosystems, Foster City, CA) on an ABI Prism 7300 Real Time PCR System.

Cellular western blotting

Cell cultures in 100 mm dishes were washed twice with PBS and scraped into 300 μ l of sample buffer. Lysates were denatured for 5 min at 95 °C, sonicated with Branson Sonifier 250 to shear DNA and centrifuged for 10 min at 16,000 rcf. Soluble proteins were quantified by Lowry's method using the D_C Protein Assay Kit (Bio-Rad, Hercules, CA). Twenty micrograms of whole cell extracts were resolved on 4–12% SDS-polyacrylamide gels and transferred onto Ready gel blotting sandwiches immunoblot PVDF membranes (Bio-Rad) using a XCell II™ Blot Module (Invitrogen). Membranes were then probed with crude SelN antibody raised in rabbit (1:500). After incubation with HRP-conjugated AffiniPure Goat Anti-Rabbit IgG (1:10,000), reactive proteins were visualized with Supersignal West Pico Chemiluminescent substrate (Thermo Fisher Scientific).

Glutathione assay in cells and zebrafish

Zebrafish and cells were tested for oxidized and reduced forms of glutathione (GSH) using a Glutathione Colorimetric Detection Kit (Thermo Fisher Scientific). Five 6 dpf zebrafish per sample were humanely euthanized and homogenized using 100 μ l of 100mM phosphate buffer, pH7. Procedure for both cell and zebrafish was continued as indicated by the manufacturer. Colorimetric reaction was measured using a plate reader every minute for 20 min.

ROS quantification in C2C12 cells

Intracellular ROS was measured using CM-H₂DCFDA (Invitrogen). Briefly 3 samples per group of cells were detached by trypsin and washed in PBS and spun down. The cell pellets were then resuspended in 100 μ l of PBS containing 5 μ M CM-H₂DCFDA and incubated at 37°C for 15 min. Cells were then washed with PBS and resuspended in 0.5 ml of PBS. 10,000 cells per sample were analyzed for fluorescence using Becton Dickinson FACS-Vantage SE flow cytometer. The data were analyzed using Flowjo software (Tree Star, Inc., OR).

Carbonylation and nitrosylation assay

Total carbonylated proteins were quantified using Oxy-Blot Protein Oxidation Detection Kit (Millipore, Billerica, MA) following manufacturer's instructions using 15 μ g of total protein detected with rabbit anti-DNP antibodies (Invitrogen) at 1:1,000 and HRP-conjugated AffiniPure

Goat Anti-Rabbit IgG (1:10,000). Total S-nitrosylated proteins were measured using an S-nitrosylated Protein Detection Assay Kit (Cayman Chemical Company, Ann Arbor, MI). Both carbonylated and S-nitrosylated proteins were detected using Supersignal West Pico Chemiluminescent substrate (Thermo Fisher Scientific) and quantified by scanning the gels on a ChemiDoc XRS gel documentation system and analyzed using Quantity One software v. 4.5.2 (Bio-Rad). The top of each gel was defined as Relative front (Rf) = 0 and the bottom as Rf = 1. Repeated intensity measurements were made down the center of each lane at intervals of Rf = 0.0043.

Generation of *Selenon* knock out C2C12 cell lines

Using CRISPR-Cas9 system we established two new *Selenon*-null C2C12 myoblast lines. These lines were generated independently. One resulted in mutations in exon 5 of the *Selenon* gene, and the second one in exon 3. This was achieved by using lipofectamine and transfecting with LentiCRISPRv2 plasmids. The following sequences were used to clone gRNAs coding regions in the plasmids for *selenon* exon 3 or exon 5 gRNAs: Ex3-F 5'-caccgTATGGTAAGAGTCTCCTCGC-3', Ex3-R 5'-aacGCGAGGAGACTCTTACCATAc-3', Ex5-F 5'-caccgGGCAAAGCGGGTCTTCACGA-3', and MouseSepnEx5-gRNA-R 5'-aacTCGTGAAGACCCGCTTTGCCc-3'. Puromycin antibiotic was used to select for transfected cells and single cells were isolated and grown individually. New single colonies were expanded and sequenced to identify null mutations.

Primary myoblast isolation

To isolate primary myoblasts from our *SELENON*-CM mouse model, we euthanized and dissected the quadriceps muscles from 3-month-old mice. We then followed myoblast isolation protocol by Shahini et al., 2018 [34]. Myoblasts were frozen in 10% DMSO growth media and utilized up to 7 passages.

Seahorse (Agilent) metabolic function in myotubes and zebrafish embryos

To test metabolic function in C2C12 cells, primary cell lines, and 24 h post fertilization (hpf) zebrafish embryos we used the Seahorse XFe96 Analyzer by Agilent (Santa Clara, CA) following manufacturer instructions. For zebrafish experiments we placed a single dechorionated embryo in XFe96 Spheroid Microplate per well in Danio water and measured real time metabolic activity using the following protocol: Port A injected a final concentration of 12.5 μ M oligomycin, port B injected 2 μ M FCCP and 1mM sodium pyruvate, port C injected 10 μ M rotenone and antimycin-A, and port D injected 5mM 2-deoxyglucose. Timing between measurements was:

2 min mixing, 1 min wait, and 2 min measure, repeated 5 times for baseline and after each port injection.

C2C12 cells and primary myoblasts, cells were seeded onto XFe96 Cell Culture plates pre-coated with 0.09 mg/ml Matrigel (Corning Inc., Corning, NY). The following day cells were differentiated using 2% horse serum media for C2C12 and according to [34] instructions for primary cells, for 5 days. Myotubes were then tested in the Seahorse XFe96 Analyzer using the following protocol: Port A injected a final concentration of 1.5 μ M oligomycin, port B injected 1.5 μ M FCCP and 1mM sodium pyruvate, port C injected 2.5 μ M rotenone and 1.5 μ M antimycin-A, and port D injected 5mM 2-deoxyglucose. Timing between measurements was: 2 min mixing, 1 min wait, and 2 min measure, repeated 3 times except for measurements after port B, which were repeated 5 times. Immediately upon assay completion, leftover media was carefully removed, and cells were lysed for creatine kinase assay and protein concentration for normalization. Colorimetric creatine kinase activity assay (Abcam, Cambridge, UK) was performed after each Seahorse assay followed by BCA protein assay (Thermo Fisher Scientific).

Ultrastructure imaging of zebrafish using transmission electron microscopy

Six dpf zebrafish larvae were euthanized and placed in glutaraldehyde fixative diluted in fish water at a 1:1 ratio. After 2 days, fish were sectioned and prepared for transmission electron microscopy (TEM) imaging using JEOL 1200EX-80 kV microscope. Slow twitch fibers were identified as adjacent to the skin and myofibrils were imaged at 2500X. At least 13 images were recorded for each fish and mitochondria areas were quantified using Image J software.

Results

Zebrafish models of *SELENON*-CM show null or reduced expression of SelN

Using CRISPR-Cas9 technology we established three independent zebrafish lines with different mutations in exon-2 of the *selenon* gene (NM_001004294.4). Two mutations, *selenon*: c.197-200del (ZFIN zebrafish line *selenon*^{cl502}) and c.199-203del (*selenon*^{cl503}), remove four and five base pairs respectively, leading to frameshifts p.L67RfsX57 and p.L67GfsX16 predicted to result in early truncation of the protein, representing presumptive null mutations of SelN (*selenon*-KO). The third is a 3 bp deletion, c.197-199del (*selenon*^{cl504}), leading to in-frame loss of one amino acid, p.G66VdelL67 (Fig. 1A). Three-D modeling of zebrafish wild type (WT) and p.G66VdelL67 SelN using SWISS-MODEL [35, 36] predicts disruption of an α -helix in the N-terminal domain of SelN (Supplemental Fig. 1). This suggests that the deletion of Leucine 67 affects the folding of SelN and either

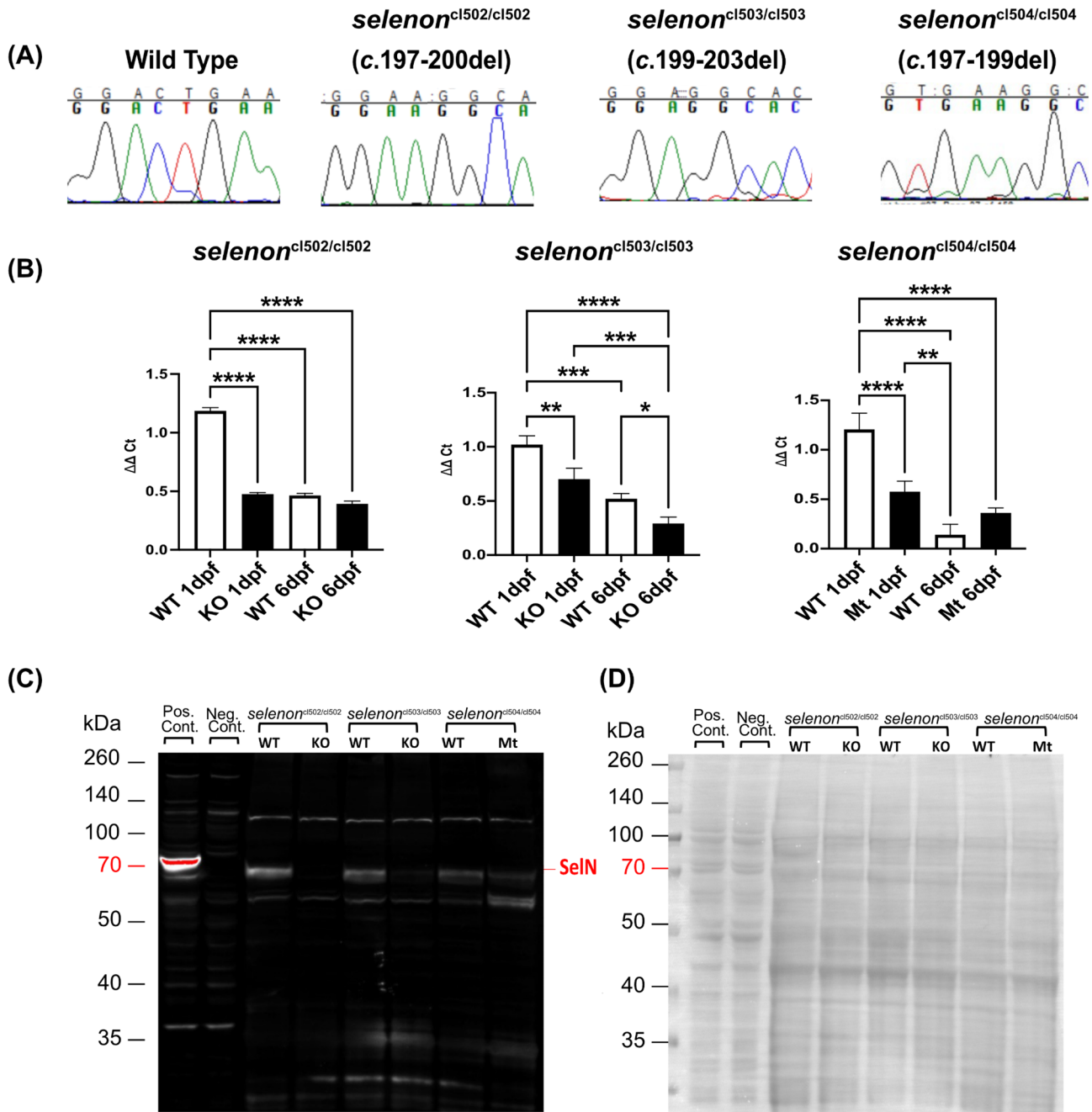


Fig. 1 Zebrafish *selenon* mutants show absent or partial expression of Selenoprotein-N. **(A)** Sanger sequencing chromatograms show analysis of the *selenon* gene exon 2 for wild type (WT), *selenon*^{c1502}, *selenon*^{c1503}, and *selenon*^{c1504} homozygotes using genomic DNA from zebrafish tail clips. **(B)** Real Time qPCR analyses show *selenon* transcript levels at 1 dpf and 6 dpf in zebrafish knock outs (KO's) and mutants (Mt): *selenon*^{c1502}, *selenon*^{c1503}, and *selenon*^{c1504} with their correspondent WT. (N=5 per group) **** $p < 0.0001$, *** $p < 0.001$, ** $p < 0.01$, * $p < 0.05$. **(C)** Western Blot analysis shows SelN expression at the predicted size of ~65 kDa in positive control (SelN-transfected HEK cells) but not in negative control (WT HEK cells). Protein lysates from 2 dpf zebrafish *selenon* mutants and their corresponding WT controls show SelN expression in all WT fish, no expression in *selenon*^{c1502} and *selenon*^{c1503}, and reduced expression in *selenon*^{c1504} mutant line. (N=30 per group) **(D)** Ponceau staining in western blot used to demonstrate equal protein loading throughout the blot

interferes with its normal function or results in reduced protein stability that may result in degradation by the cell. To assess consequences of these mutations we measured relative *selenon* transcript levels in wild type (WT)

and homozygous mutants of the three zebrafish lines at 1- and 6 dpf (Fig. 1B). The highest levels of *selenon* transcript were found in WT embryos at 1 dpf, while same age-mutant embryos showed approximately half those

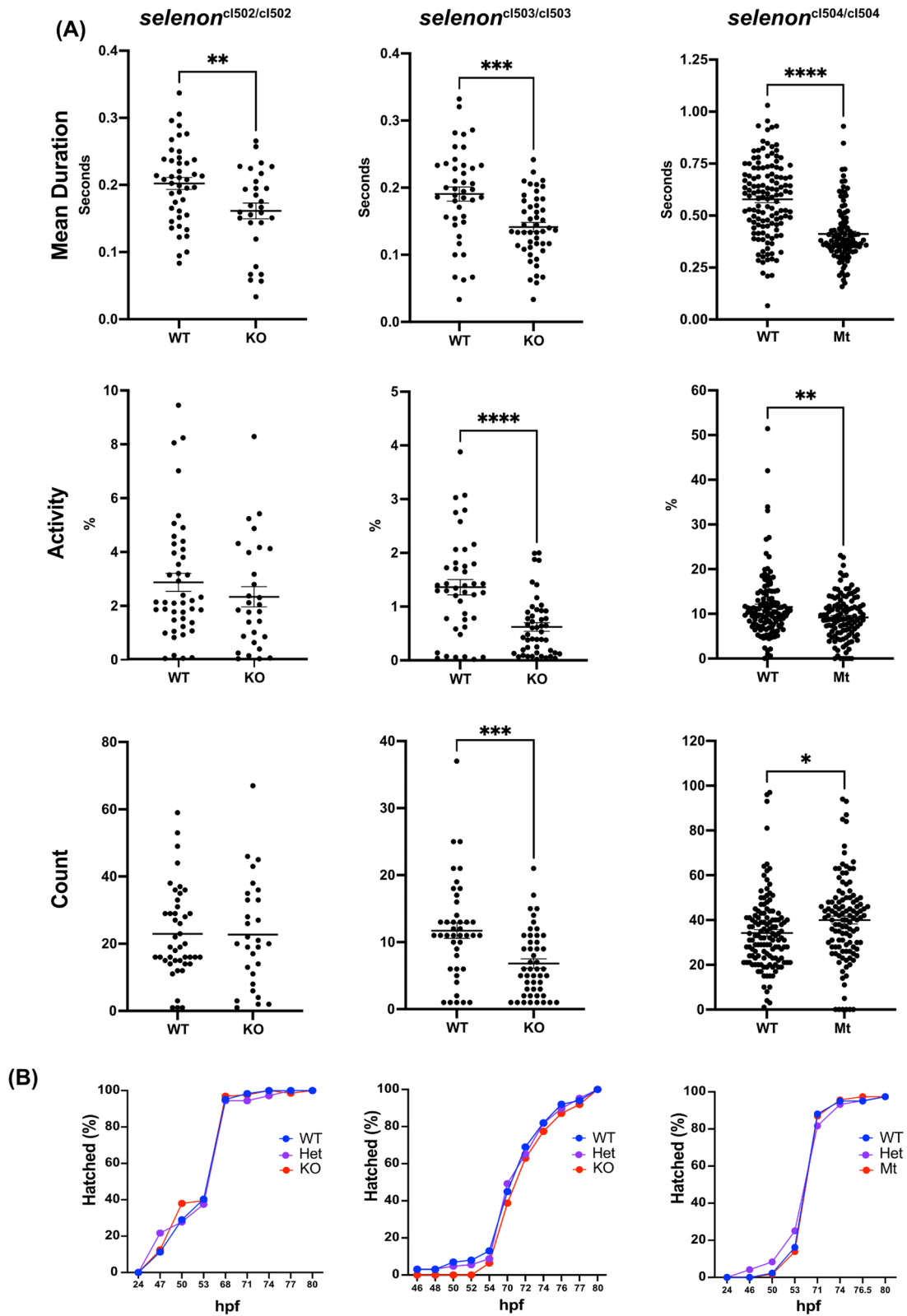


Fig. 2 (See legend on next page.)

(See figure on previous page.)

Fig. 2 Selenoprotein-N deficient zebrafish embryos present with impaired spontaneous contractions. Spontaneous tail and trunk contractions of zebrafish embryos were recorded and quantified at 24 hpf in SelN homozygous KO *selenon*^{cl502} ($N=45$ and 29), *selenon*^{cl503} ($N=43,48$), and homozygous mutant (Mt) *selenon*^{cl504} ($N=131,116$) and their correspondent WT controls. **(A)** Mean duration of spontaneous contractions, percent time of contraction activity, and total number of contractions are reported in each line. ****** = $p < 0.05$, ******* = $p < 0.01$, ******** = $p < 0.001$, ********* = $p < 0.0001$. **(B)** WT, heterozygous and homozygous embryos were observed for hatching activity and recorded up until 80 hpf ($N=41-100$ WT, $92-134$ heterozygous, and $56-93$ homozygous mutant embryos per line)

levels of expression. By 6 dpf, *selenon* expression in all lines dropped by half or more compared to 1 dpf WT embryos. Lastly, 6 dpf *selenon*-KO lines showed the same or lower transcript levels when compared to WT, while 6 dpf *selenon*^{cl504/cl504} showed a trend towards increased transcript level when compared to WT. Next, we analyzed SelN protein content in 2 dpf zebrafish (Fig. 1C, D). SelN expression was undetectable in the two frame-shifted and presumptive null lines (*selenon*^{cl502/cl502} and *selenon*^{cl503/cl503}) and apparently reduced by about 55% in *selenon*^{cl504/cl504} fish with a single amino acid deletion.

SelN deficiency in zebrafish is compatible with grossly normal development

Heterozygote matings led to expected 1:2:1 proportions of WT, heterozygous, and homozygous KO fish for all three lines. Homozygous offspring survived to at least 1.5 years of age, were fertile, and produced healthy and normal appearing offspring just as well as WT fish. Light microscopic examination of 24 hpf embryos revealed no abnormalities of body plan, or somite organization, and birefringence assays [37] at 6 dpf were also unremarkable, demonstrating normal sarcomeric organization (data not shown).

Zebrafish models of SELENON-CM exhibit reduced spontaneous contraction during embryogenesis

During zebrafish somitogenesis embryos begin to spontaneously contract their trunk and tail from 17 hpf to approximately 26 hpf [38, 39]. The frequency of these muscle contractions is dependent on motor neuron activation and this process is essential for proper axial skeletal muscle formation [40, 41]. Lesions in the hindbrain do not inhibit these contractions indicating that these events result from activation of the spinal neurocircuitry with no input from the brain [38]. Additionally, it has been shown that muscle contraction at this stage is dependent only on slow twitch fibers (mitochondrial positive fibers) with no input from fast twitch fibers [42]. Zebrafish embryo transparency allowed us to directly observe and quantify spontaneous contractions as a means to study embryonic muscle function. Fish embryos at 24 hpf were videotaped for 3 min and their spontaneous movements were later analyzed computationally. We quantified mean durations of contraction, percentage of total active time, and total numbers of contractions. *Selenon* mutants exhibited significantly decreased mean duration of contractions

across all three lines (Fig. 2A). The percentage of active time was significantly lower in the two *selenon* KO lines when compared to WT; while *selenon*^{cl504/cl504} embryos showed a trend towards decrease when compared to WT. The absolute number of contractions, on the other hand, showed no changes in *selenon*^{cl502/cl502} but was significantly reduced in *selenon*^{cl503/cl503} and significantly increased in *selenon*^{cl504/cl504}. These results indicate that the mean duration of contraction was the most consistent difference during spontaneous contractions in *selenon* mutated zebrafish embryos.

To understand whether these changes in contraction were due to delayed early zebrafish growth, we quantified hatching activity in these three lines (Fig. 2B). To do so, we generated embryos from matings of *selenon* heterozygous fish and observed the hatching activity from 3 to 5 dpf. Hatching time courses for subsequently genotyped fry of all three lines demonstrate that there are no differences between WT, heterozygous (HET), and *selenon*-KO or *selenon*^{cl504/cl504} fish. These data indicate that SelN-deficiency does not lead to hatching abnormalities or delay in zebrafish development.

Selenoprotein N-deficient zebrafish larvae show changes in swim activity

To assess motor activity during larval stages of development we tested our SelN-deficient zebrafish lines using a swim activity monitor. Six dpf larvae were evaluated using a protocol that included vibrations and light-and-dark cycles. As an example, we show the swimming activity of *selenon*^{cl502/cl502} and WT zebrafish throughout the protocol (Fig. 3A). Changes in light and vibration induced continuous swim activity in both WT and *selenon* mutant fish, but the *selenon* KO lines exhibited significant decreases in total swim activity when compared to WT, while *selenon*^{cl504/cl504} showed a trend towards decreased swim activity (Fig. 3B).

To determine whether these changes in activity were due to ultrastructural modifications in the zebrafish larvae skeletal muscle, we imaged 6 dpf *selenon*-mutants and their corresponding WT clutch-mates using transmission electron microscopy (TEM). We show representative images of WT and KO *selenon*^{cl502} skeletal muscle myofibrils (Supplemental Fig. 2). We did not identify changes in contractile structures nor presence of minicores within the myofibers. However, we quantified intermyofibrillar mitochondria areas and observed a significant increase in

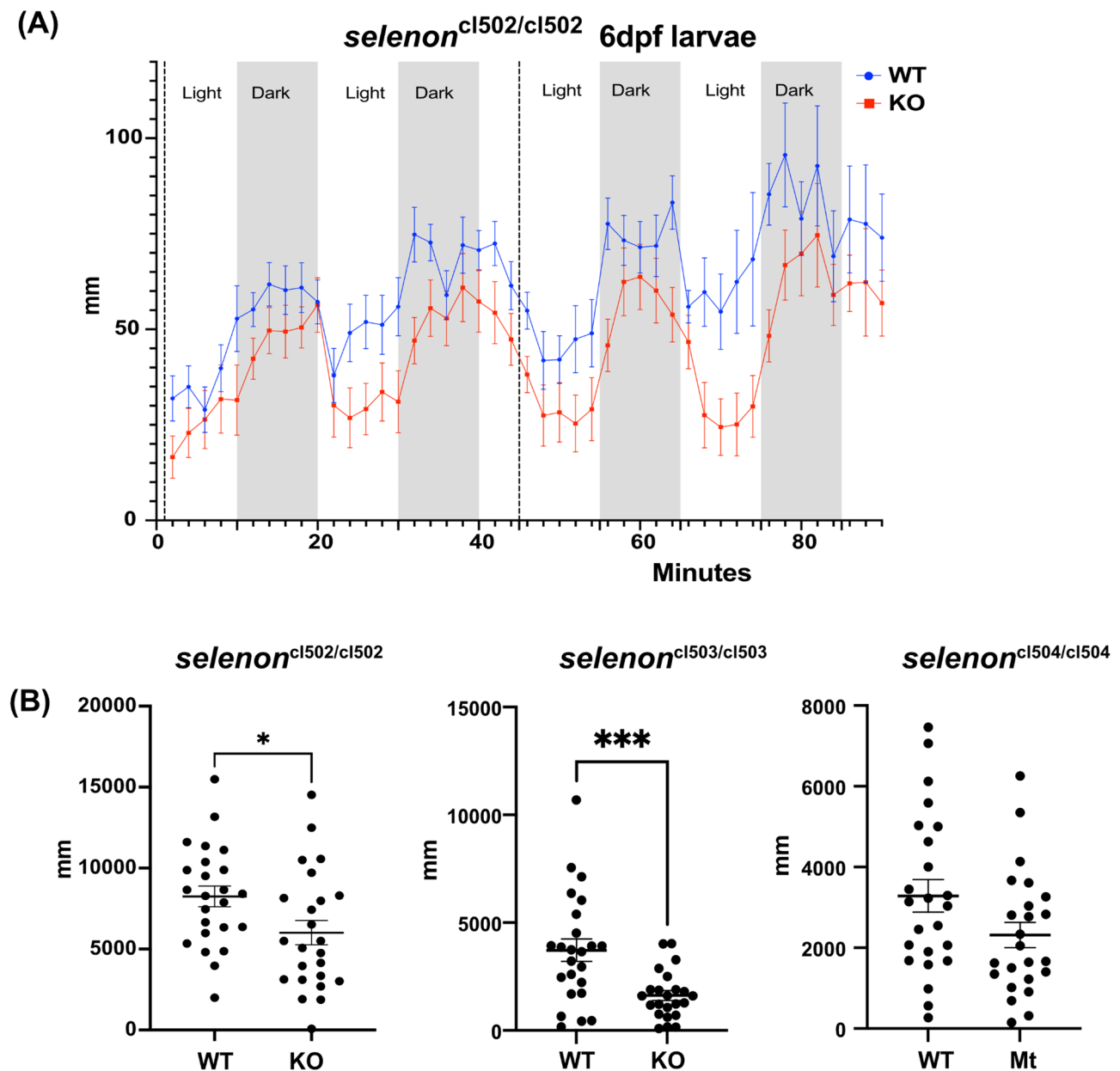


Fig. 3 *Selenon*-deficient zebrafish larvae show decreased activity. **(A)** 6 dpf WT (blue) and homozygous *selenon*-KO *selenon*^{cl502/cl502} (red) zebrafish larvae were tested for swim activity using an activity monitor and a 90-minute protocol that included vibration (dotted lines) and cycles of alternating light (non-shaded areas) and dark (shaded areas) periods. **(B)** Quantification of activity assays of WT and homozygous *selenon*-mutant lines shows decreased total distance swum in *SelN*-deficient zebrafish larvae when compared to their corresponding WT controls ($N = 24$). $^{**} = p < 0.05$, $^{****} = p < 0.001$

SelN-KO fish lines when compared to WT and a decrease in *selenon*^{cl504/cl504} when compared to WT.

Analysis of gene expression in a zebrafish single cell atlas identifies correlation between *Selenon* gene expression and ER oxidoreductase activity in skeletal muscle precursor cells

To understand patterns of *selenon* expression during zebrafish early development we consulted single cell RNAseq atlases by Wagner et al. 2017 and Farnsworth

et al., 2020 [24, 43]. The Wagner publication sequenced cell transcripts from 1 to 24 hpf, while the Farnsworth publication sequenced cells from 1 dpf to 5 dpf. *Selenon* patterns of expression in both atlases revealed peak expression at 24 hpf in both notochord and tailbud presomitic mesoderm cells (PSM), which are precursors of skeletal muscle. This is consistent with previous in vitro hybridization studies in mouse and zebrafish embryos [16, 23–25]. Based on this, we focused our attention on Wagner's atlas tailbud PSM cell clusters. In this atlas, over

90,000 cells' transcriptomes were sequenced throughout zebrafish embryonic development. These transcriptomes were then clustered and constructed in a tree-like diagram that branches into the different trajectories of zebrafish cell differentiation (Supplemental Fig. 3A). The analysis reveals incremental *selenon* expression in tailbud PSM cells in 6, 8, 10, 14, 18, and 24 hpf cell clusters. The transcriptome data from the highlighted PSM clusters was used to identify correlations between expression of *selenon* and other genes. Weighted correlation networks were generated using the WGCNA method with the transcriptome data (see Methods) and two modules, 'antiquewhite1' (4516 genes) and 'firebrick2' (240 genes) were selected based on target *selenon* gene having significant correlation with p-values < 0.05 (Supplemental File 3). Using Cytoscape, 3339 genes from 'antiquewhite1' and 168 from 'firebrick2' were visualized as *selenon* positively associated gene networks. All co-expressed genes from significant modules 'antiquewhite1' and 'firebrick2' were subjected to pathway and gene ontology (GO) enrichment analysis. Following pathway enrichment, GO analysis revealed pathways involved in molecular functions, cellular components, and biological processes. Due to its relevance to SelN's oxidoreductase activity, we focused on the 'oxidoreductase activity acting on peroxide as an acceptor' GO pathway in 'antiquewhite1' module. Supplemental Table 1 lists the genes included in this group organized by weight of correlation to *selenon*. To further explore the genes listed in Supplemental Table 1, we utilized Ingenuity Pathway Analysis (IPA) to identify potential pathways involved with SelN function. We show IPA identified pathways upregulated with SelN organized by statistical significance (Supplemental Fig. 3B). "Glutathione Redox Reactions I" and "Apelin Adipocyte Signaling Pathway" head the list with positive z-scores indicating gene upregulation. We focused on "Glutathione Redox Reactions I" which involves 4 redox genes: *gpx7*, *gpx8*, *gpx4a* and *gpx1a* (Supplemental Fig. 3C).

Glutathione redox homeostasis is altered in SelN-deficient cell models

Based on our observation using the single cell RNAseq zebrafish atlas, we hypothesized that co-expression of *selenon* with components of the glutathione redox pathway may reflect functional relationships. To test this, we induced *Selenon* transcript knock down in C2C12 mouse myoblasts using shRNA. *Selenon* transcript levels in three C2C12 knock down (KD) cell lines were reduced to ~20% in line KD1, ~10% in KD8 and ~60% in KD3 relative to parallel control lines (Supplemental Fig. 4). By western blotting, SelN protein expression was overall reduced in KD1 and KD8 cell lines, relative to controls.

Next, we assayed our SelN-KD cell lines and *SELENON*-CM zebrafish models for glutathione (GSH) redox

states. In our cell lines, we quantified the ratio between oxidized (GSSG) and reduced (GSH_{free}) forms of GSH. This ratio allowed us to identify global changes in glutathione redox state. Results show that the glutathione ratio ($GSH_{free}/GSSG$) was significantly downregulated in both KD1 and KD8 and maintained the same trend towards decreased ratio in KD3 when compared to control (Fig. 4A). This suggests that GSH redox ratio is sensitive to downregulation of the SelN protein in C2C12 myoblasts.

Additionally, we tested $GSH_{free}/GSSG$ ratios in our zebrafish models of *SELENON*-CM at 6 dpf. Results showed no significant differences between any SelN-deficient fish line and their matched WT controls (Fig. 4B). This suggests that in contrast with cell models, zebrafish GSH redox state is not sensitive to levels of SelN protein.

SelN-deficient myoblasts exhibit increased oxidative stress

To determine whether SelN downregulation induces oxidative stress, we quantified the presence of reactive oxygen species (ROS) in SelN-KD and control C2C12 cells. To do so we used CM-H2DCFDA as a general oxidative stress indicator in our cell lines and flow cytometry. Results show a shift towards increased ROS in both the KD1 and KD8 when compared to control cells (Fig. 5A). We also show quantification of the mean fluorescence per group which shows a significant increase in KD1 and KD8 when compared to control cells (Fig. 5B). To determine whether the higher levels of ROS in SelN-deficient cells are associated with activation of oxidative damage or modification, we quantified levels of carbonylation and nitrosylation in each line. Both SelN-KD lines showed significant increases in levels of carbonylated proteins relative to controls (Fig. 5C). Similarly, we show an increase in nitrosylated proteins in SelN-KD cell lines when compared to control cells (Fig. 5D). These data indicate that SelN-deficiency induces high levels of oxidative stress resulting in irreversible protein oxidation.

SelN null myotubes show impaired metabolism

Given the correlation between SelN deficiency and mitochondrial abnormalities, we hypothesized that *Selenon*-KO myoblasts may present metabolic impairment. To test this idea, using CRISPR-Cas9 technology we independently created two new C2C12 myoblast lines with homozygous *Selenon* null mutations in exon 3 and exon 5. Additionally, we isolated primary quadriceps myoblast cell lines from our mouse model of *SELENON*-CM, which has a homozygous null mutation in exon 8 [27]. Each line was tested with a matched WT cell line for comparison. Immunoblot analysis of SelN protein confirmed its absence in both C2C12 cell lines as well as in our mouse *Selenon*-KO quadriceps primary cells (Fig. 6A).

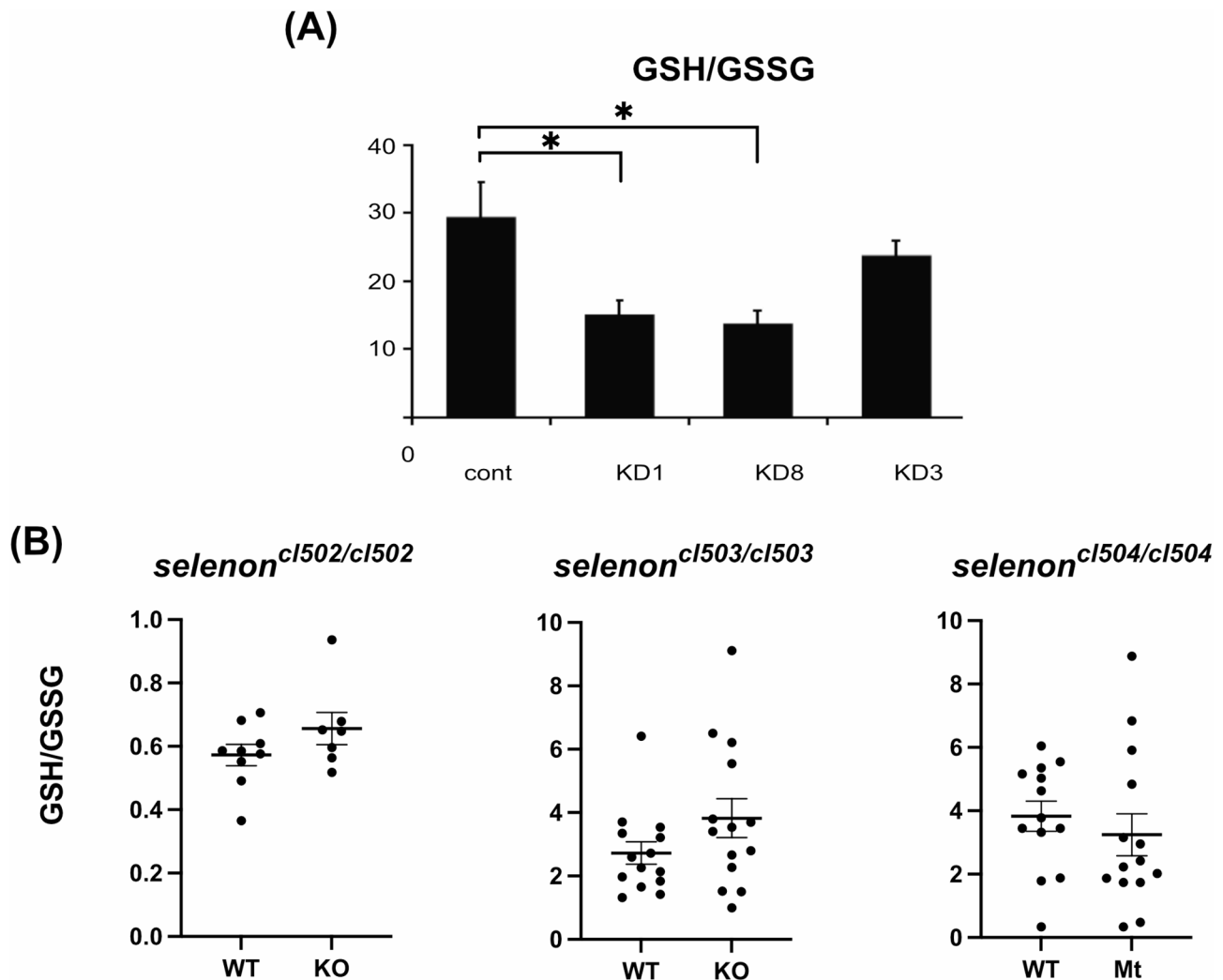


Fig. 4 Glutathione homeostasis is altered in cell models of *SELENON*-CM. **(A)** *Selenon* Knock Down (KD) cell lines show decreased glutathione ratio (GSH/GSSG) when compared to WT control. **(B)** GSH/GSSG ratio were measured in 6 dpf *selenon*^{cl502} ($N=9$ and 7), *selenon*^{cl503} ($N=14$), and *selenon*^{cl504} ($N=13$ and 14) zebrafish lines. $^{**} = p < 0.05$, $^{***} = p < 0.01$, $^{****} = p < 0.001$

To test for changes in metabolism in our cell lines, we used the Seahorse cell respirometer to measure Oxygen Consumption Rate (OCR) and Extra Cellular Acidification Rate (ECAR). We used increasing concentrations of exon 5 *Selenon*-KO and WT myoblasts. Cells were then differentiated into myotubes and measured for OCR and ECAR. After completion, we measured creatine kinase activity and protein concentration in each well for normalization of differentiation and cell number respectively. Using OCR values, we calculated basal levels of cellular respiration, ATPase activity, maximal respiration capacity, and non-mitochondrial oxygen consumption. At the same time, with ECAR levels we calculated basal glycolysis, maximal glycolysis levels, and non-glycolytic acidification (data not shown). Results show an overall decrease in all OCR and ECAR parameters in the *Selenon*-KO myotubes when seeded at 20,000 cells per well

and differentiated for five days (Fig. 6B). We show quantification of basal respiration and basal glycolysis in different cell confluency groups (from 5,000 to 20,000 cells per well). However, *Selenon*-KO myotubes exhibited 50% decreases in OCR and 61% decrease in ECAR compared to WT only when seeded at 20,000 cells/well (Fig. 6C, D). Additionally, primary quadriceps myotubes from *Selenon*-KO mice exhibited 78% reduction in OCR and 60% reduction in ECAR when compared to WT at 20,000 cells per well. Lastly, differentiated C2C12 cells with exon 3 *Selenon*-KO had 60% reduction in OCR and 61% reduction in ECAR at 20,000 cells per well. These data indicate that SelN-deficiency triggers a metabolic deficiency at high myotube confluency. These observations further support mitochondrial involvement in *SELENON*-CM.

To test whether similar effects in metabolism might be detectable in vivo in our zebrafish models of

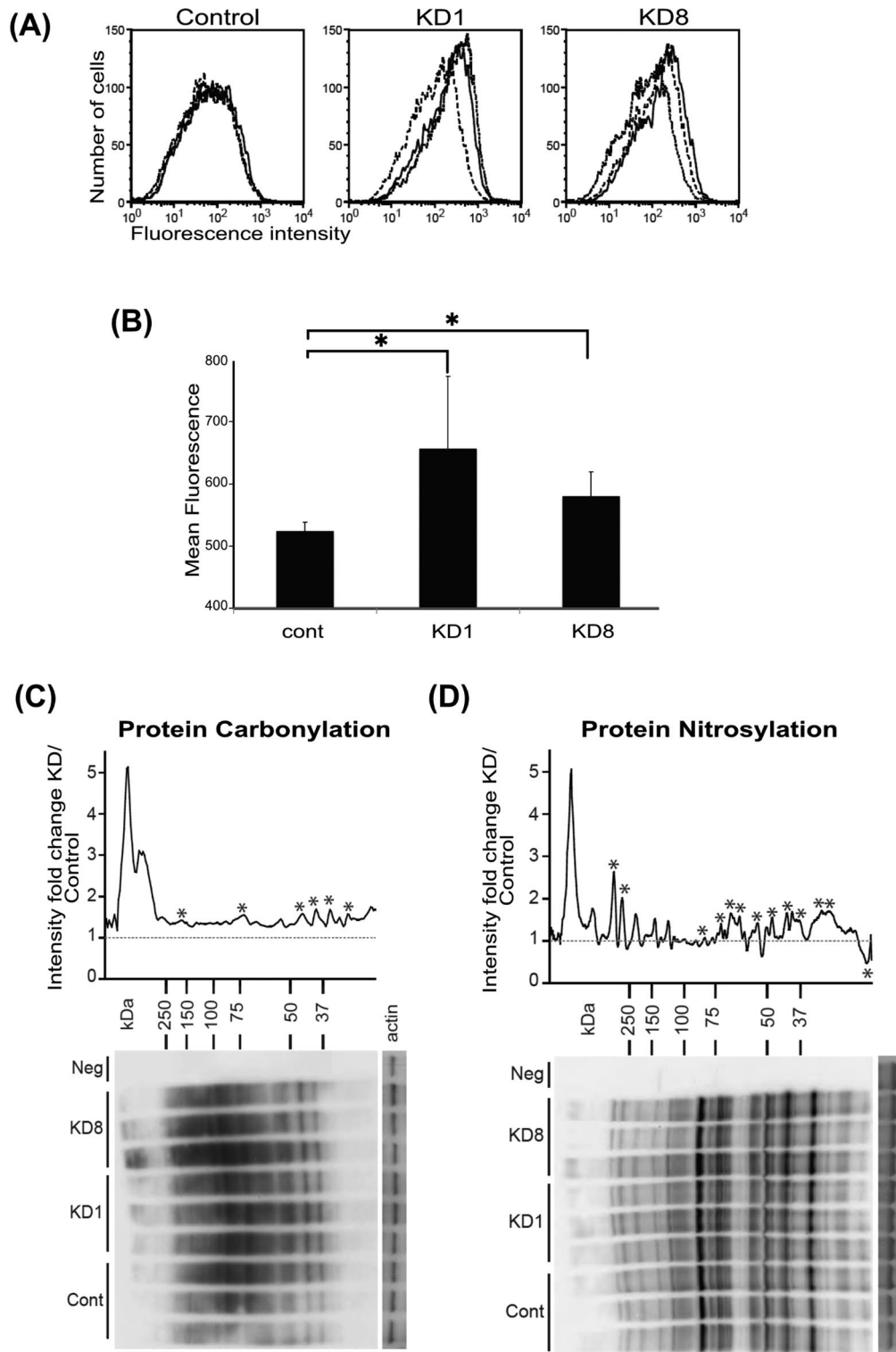


Fig. 5 *Selenon* knock down cells present increased ROS levels when compared to control. **(A)** Flow cytometry assay of CM-H₂DCFDA stained cells to measure ROS levels in *selenon* knock down (KD1 and KD8) and WT control cells. **(B)** Quantification of fluorescence from **(A)** reveals significant increase of ROS levels in *selenon* KD cell lines when compared to control. **(C)** Immunoblotting of protein carbonylation and **(D)** nitrosylation demonstrate increased levels in *selenon* KD when compared to control cells

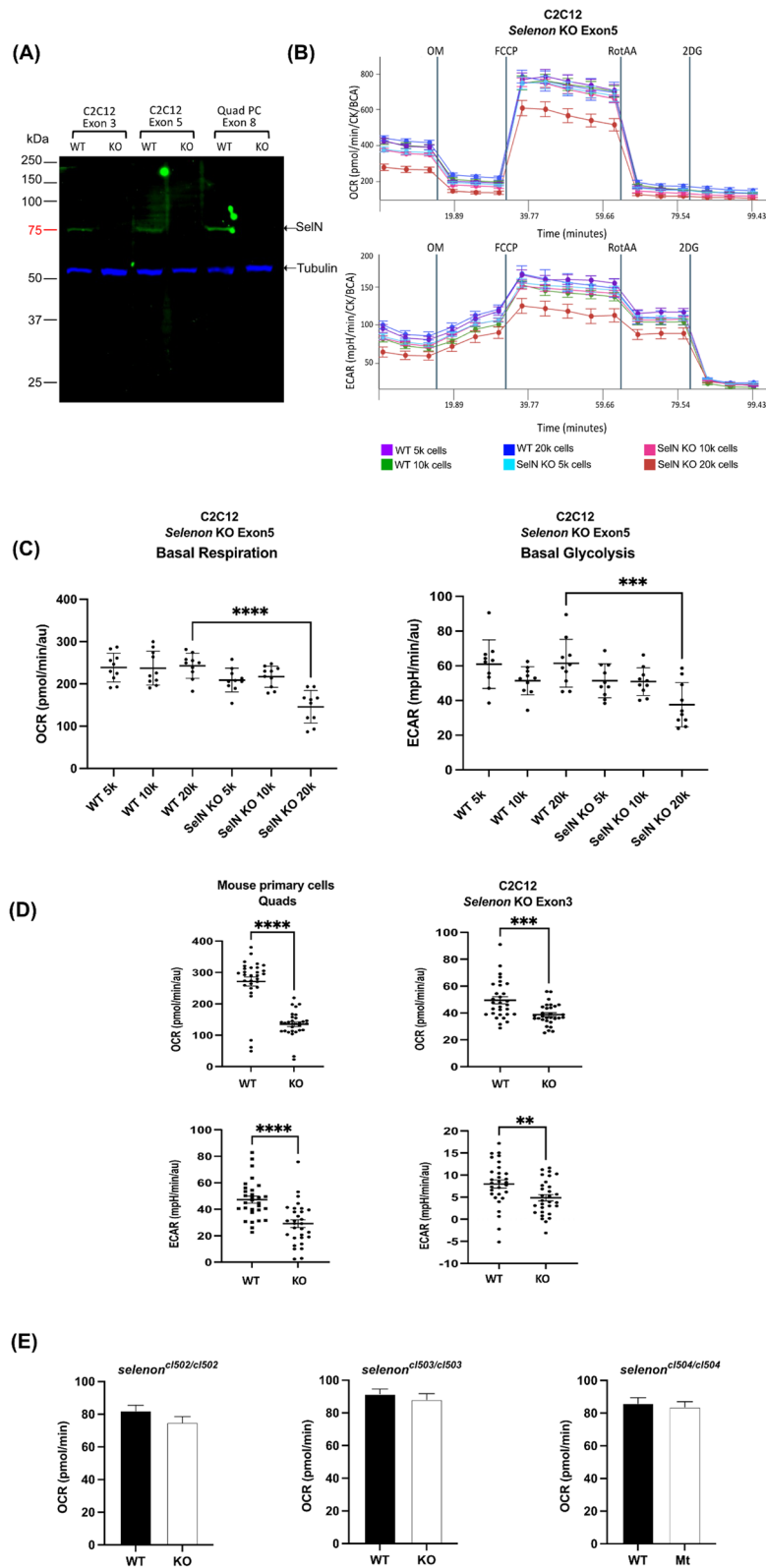


Fig. 6 (See legend on next page.)

(See figure on previous page.)

Fig. 6 Selenoprotein-N null myoblasts show impairment in metabolism after differentiation at high cell seeding confluency. **(A)** Immunoblot shows absence of ~65 kDa SelN in three *selenon*-null myoblast lines: C2C12 Exon 3, C2C12 Exon 5, and mouse quadriceps primary cells (Quad PC). α -Tubulin was used as a loading control and is present at ~52 kDa in all lines. **(B)** Results from seahorse cell respirometer show changes in Oxygen Consumption Rate (OCR) and Extra Cellular Acidification Rate (ECAR) parameters at different cell plating densities of *selenon*-null C2C12 Exon 5 cells. **(C)** Quantification of OCR and ECAR in increasing concentrations of C2C12 *selenon*-null exon 5 myoblasts show significant differences when compared to wild type only at 20,000 cell density ($N=10$). **(D)** Quantification of basal OCR and ECAR in C2C12 *selenon*-null exon 3 and one mouse quadriceps primary *selenon*-null cell lines shows impaired metabolism in KO myoblasts when compared to WT at 20,000 cell density ($N=30$). **(E)** Quantification of basal OCR in three 1 dpf *selenon*-mutant zebrafish embryos show no differences in metabolism in mutants when compared to WT ($N=48$). $*** = p < 0.01$, $**** = p < 0.001$, $***** = p < 0.0001$

SELENON-CM, we tested 1 dpf embryos using the cell respirometer. We replicated the Seahorse protocol used for myotubes and tested homozygous embryos for each zebrafish line. In contrast to cultured and differentiated murine myotubes we did not detect measurable differences in respiration levels between WT and *selenon*-mutant embryos of any of the three independent lines (Fig. 6E).

Discussion

A major challenge in the study of *SELENON*-CM has been that, despite the significant disease burden in patients afflicted with this condition, cellular and animal models do not exhibit clear phenotypes [26–28]. Although molecular and biochemical abnormalities related to SelN deficiency have been well documented, difficulties in demonstrating readily assayable clinical phenotypes have inhibited therapy development. Here we present three new zebrafish models for the study of *SELENON*-CM. Unlike the murine KO models, both SelN-deficient fish and human *SELENON*-CM patients exhibit signs of early developmental abnormalities (spontaneous coiling and reduced activity in fish, and midline facial defects, congenital contractures and neonatal hypotonia in humans). SelN-deficiency is compatible with normal lifespans in all three species, but only humans develop clinically demonstrable muscle dysfunction in the absence specific stressors such as frequent forced swimming or treadmill exercise in the case of the mouse models [27, 28]. Although the mice exhibit a developmental defect in pulmonary alveolar structure [27], this appears distinct from the pulmonary insufficiency secondary the respiratory muscle dysfunction seen in humans [5, 6], and there is no analogous deficiency observable in the fish. Only humans develop the characteristic skeletal muscle pathology that defines the condition.

Quantitative RT-PCR analysis of *selenon* mRNA levels at 24 hpf and 6 dpf in our lines revealed highest levels at 24 hpf in WT fry, suggesting an important role of *selenon* expression during early embryonic development. Frame-shift-mutant fish had lower levels of steady state *selenon* mRNA at both 24 hpf and 6 dpf, perhaps reflecting the consequences of nonsense-mediated decay. However, our in-frame mutant fish showed increased *selenon* mRNA

expression at 6 dpf, when compared to WT. This is consistent with a previous study by Maiti et al., 2009, where they measured SelN protein and *SELENON* transcript levels in biopsies from *SELENON*-CM patients. They found that when protein levels were null, transcript level was reduced compared to control [44]. However, when SelN protein levels were reduced, transcripts were elevated in patient samples when compared to controls, possibly reflecting a potential compensatory response.

Measurement of spontaneous contractions (coiling) in zebrafish is a sensitive functional assay to measure embryonic muscle function [45, 46]. These contractions are mediated by slow-twitch oxidative fibers [42] rich in mitochondrial content [47, 48]. All three *selenon* mutant lines exhibited significantly decreased mean durations of contraction when compared to WT (Fig. 2). Additionally, the percent of activity was significantly reduced in two *selenon* mutants and showed a trend towards decrease in a third line (*selenon*^{cl502}). Taken together in light of the Seahorse assay results indicating abnormal mitochondrial function in SelN-deficient cells, these data support the notion that *SELENON*-CM results from significant defects in mitochondrial function.

Ultrastructural analysis of our zebrafish skeletal muscle did not identify any major changes to the myofibrillar ultrastructure or presence of multimimicore, however we found differences in mitochondrial content associated with *selenon* genotype. Total mitochondrial area was slightly increased in both *selenon*^{cl502/cl502} and *selenon*^{cl503/cl503} lines, and decreased in *selenon*^{cl504/cl504} fish at 6 dpf when compared to WT. These changes in skeletal muscle mitochondria along with changes in swim activity further support the idea that SelN plays a role in skeletal muscle mitochondrial function during zebrafish early growth.

Given our evidence that SelN may play an important role in zebrafish embryos at 24 hpf, we performed a bioinformatic analysis using previously published single cell RNAseq atlas [24]. We identified cell clusters belonging to presomitic mesoderm (PSM) cells that showed increasing expression of *selenon* peaking at 24 hpf (Supplemental Fig. 3A). This, along with our previous functional data in 24 hpf embryos, point at an important role for SelN in early axial muscle development, and may be a contributing factor to the later development of axial

weakness and spinal deformities that are characteristic of *SELENON-CM* in human patients.

Gene ontology and pathway analysis from PSM cluster suggest a strong correlation between *selenon* expression, and genes involved in glutathione redox reactions signaling pathways (Supplemental Fig. 3B-C). This is consistent with previous data implicating a role of SelN in redox reactions through the glutathione pathway [17, 19, 20].

To extend these observations we generated shRNA-induced *Selenon* knock down C2C12 cell lines (*Selenon-KD*) and quantified glutathione redox ratios ($GSH_{free}/GSSG$) in control versus *Selenon-KD* cells, demonstrating a decrease in ratio proportional to their decrease in *selenon* expression (Fig. 4A). Decreased levels of $GSH_{free}/GSSG$ can be interpreted as increasing concentration of oxidized glutathione when compared to the free available reduced glutathione. This happens in response to increased oxidative stress in the cells. These data may indicate a direct correlation between *selenon* expression and glutathione homeostasis in response to increased oxidative stress in myoblasts.

Additionally, we tested glutathione homeostasis in our *SELENON-CM* zebrafish models at 6 dpf (Fig. 4B). In contrast with C2C12 cells, we found that the redox GSH ratios in the three lines were not significantly different when compared to their WT lines. These data may indicate that SelN-deficient zebrafish have a heightened ability to adapt their GSH redox ratio when compared to isolated myoblasts.

To test whether oxidative stress is elevated in SelN-deficient myoblasts, we measured reactive oxygen species (ROS) (Fig. 5A-B), protein carbonylation (Fig. 5C-D) [49], and protein nitrosylation. Our results show that ROS, protein carbonylation and nitrosylation were elevated in our *selenon-KD* cell lines. This is consistent with a previous study showing increased protein carbonylation in *SELENON-CM* patient myoblasts [20], supporting the concept that SelN plays a direct role in oxidative stress response in myoblasts.

The presence of minicores in muscle biopsies and impaired metabolic presentation in patients, suggest a direct relationship between SelN and mitochondrial function. However, mitochondrial abnormalities are a common secondary feature of muscle diseases. Here we demonstrate a direct relationship between mitochondrial dysfunction and SelN deficiency in muscle cells. When plated at high densities, assays of both basal respiration (OCR) and basal glycolysis (ECAR) revealed reduced metabolic activity in two independently derived *Selenon* KO C2C12 myoblast lines, as well as in primary myoblasts from our *Selenon* KO mouse model (Fig. 6A-D). This may indicate that SelN's role becomes more important during increased cellular stress. Being that we have previously shown that SelN may have a direct impact

in oxidative stress, these data suggest a model whereby SelN-deficient oxidative stress leads directly to impaired mitochondrial function followed by changes in glycolysis. Interestingly, we failed to detect similar metabolic changes in 24 hpf zebrafish embryos. This may indicate that metabolism is not impacted during somitogenesis perhaps due to the preponderance of fast oxidative myofibers in zebrafish and their reliance on glycolysis as primary source of energy [50, 51].

Conclusions

The present data provide new insights into the role of SelN in early embryonic development and provide the basis for new potential assays for drug and other therapeutic development. Further studies of mitochondrial structure and function in SelN-deficient cells may provide a cellular morphological phenotype that might be of use in a cell painting type assay for drug screening [52]. Assays of spontaneous coiling and motor activity in zebrafish embryos and fry may have further utility for moderate throughput drug screens and in vivo proof of concept for other developing therapeutic modalities.

Abbreviations

SELENON-CM	SELENON-Congenital Myopathy
SelN	Selenoprotein-N
RSMD	Rigid Spine Muscular Dystrophy
ER/SR	Endo/sarcoplasmic reticulum
MAMs	Mitochondrial Associated Membranes
Selenon-KO	Selenon knock out
WT	Wild Type
Dpf	Days post fertilization
Hpf	Hours post fertilization
HET	Heterozygous
TEM	Transmission electron microscopy
RNAseq	RNA sequencing
PSM	Presomitic Mesoderm Cells
GO	Gene Ontology
IPA	Ingenuity Pathway Analysis
shRNA	Short hairpin RNA
KD	Knock down
GSH	Glutathione
GSSG	Oxidized glutathione
GSH_{free}	Reduced glutathione
ROS	Reactive Oxygen Species
OCR	Oxygen Consumption Rate
ECAR	Extra Cellular Acidification Rate
NO	Nitric Oxide

Supplementary Information

The online version contains supplementary material available at <https://doi.org/10.1186/s13395-025-00376-4>.

Supplemental Figure Legends and Table S1

Supplemental Figure 1

Supplemental Figure 2

Supplemental Figure 3

Supplemental Figure 4

Supplemental File 1 - Embryo grid

Supplemental File 2 - Zantiks MatLab script

Supplemental File 3 - antiquewhite1 & firebrick2 module genes

Acknowledgements

Thanks to Elizabeth Griffin for outstanding technical assistance during a summer internship. The authors would also like to acknowledge helpful support and advice from Louise Trakimas of the Electron Microscope Core at Harvard Medical School, as well as Shanelle Kohler from Zantiks Ltd. Electron Microscopy Imaging, consultation and /or services were performed in the HMS Electron Microscopy Facility, and we would also like to acknowledge the Zebrafish Facility at Boston Children's Hospital for their continuous care of our fish.

Author contributions

PB-F contributed with conceptualization, methodology, validation, formal analysis, investigation, and writing- original draft preparation of this article. BM contributed with conceptualization, methodology, formal analysis, investigation, review and editing of manuscript. WL contributed with investigation. BI contributed with implementation of computer code, formal analysis, methodology, data curation, and reviewing and editing manuscript. LS contributed with conceptualization, implementation of computer code, data curation, supervision, and reviewing and editing manuscript. ECT contributed with investigation. SR and PS contributed with funding acquisition, reviewing, and editing manuscript. AHB contributed with funding acquisition, project administration, supervision, writing, review and editing, methodology, and conceptualization.

Funding

This work was funded by generous philanthropic support from the Lee and Penny Anderson Family Foundation, Jonathan and Deborah Parker and the Giving Strength Fund, and MDA602235 from the Muscular Dystrophy Association (USA). Support for molecular genetic analyses was provided by the Boston Children's Hospital Intellectual and Developmental Disabilities Research Center Molecular Genetics Core Facility supported by P50HD105351 from the Eunice Kennedy Shriver National Institute of Child Health and Human Development of NIH. PB-F was supported by Developmental Neurology Training Grant T32NS007473 from the National Institute of Neurological Disorders and Stroke of NIH.

Data availability

All relevant data can be found within the article and its supplementary information.

Declarations

Competing interests

AHB receives consulting income from Kate Therapeutics, Astellas Pharma, Roche Pharmaceuticals, GLG Inc, and Guidepoint Global, and has equity in Kate Therapeutics and Kinea Bio. For all other authors no competing interests are declared.

Received: 13 August 2024 / Accepted: 25 February 2025

Published online: 15 March 2025

References

- Moghadaszadeh B, Petit N, Jaillard C, Brockington M, Roy SQ, Merlini L, et al. Mutations in SEPN1 cause congenital muscular dystrophy with spinal rigidity and restrictive respiratory syndrome. *Nat Genet.* 2001;29:17–8.
- Ferreiro A, Quijano-Roy S, Pichereau C, Moghadaszadeh B, Goemans N, Bönnemann G, et al. Mutations of the Selenoprotein N gene, which is implicated in rigid spine muscular dystrophy, cause the classical phenotype of multimimicore disease: reassessing the nosology of early-onset myopathies. *Am J Hum Genet Cell Press.* 2002;71:739–49.
- Witting N, Werlauff U, Duno M, Vissing J. Phenotypes, genotypes, and prevalence of congenital myopathies older than 5 years in Denmark. *Neurol Genet.* 2017;3:140.
- Bouman K, Groothuis JT, Doorduyn J, van Alfen N, ten Udink FEA, et al. Natural history, outcome measures and trial readiness in LAMA2-related muscular dystrophy and SELENON-related myopathy in children and adults: protocol of the LAST STRONG study. *BMC Neurol.* 2021;21:313.
- Silwal A, Sarkozy A, Scoto M, Ridout D, Schmidt A, Laverly A, et al. Selenoprotein N-related myopathy: a retrospective natural history study to guide clinical trials. *Ann Clin Transl Neurol.* 2020;7:2288–96.
- de Visser M. Late-onset myopathies: clinical features and diagnosis. *Acta Myol Myopathies Cardiomyopathies Off J Mediterr Soc Myol.* 2020;39:235–44.
- Clarke NF, Kidson W, Quijano-Roy S, Estournet B, Ferreiro A, Guicheney P, et al. SEPN1: associated with congenital fiber-type disproportion and insulin resistance. *Ann Neurol.* 2006;59:546–52.
- Ferreiro A, Ceuterick-De Groote C, Marks JJ, Goemans N, Schreiber G, Hanefeld F, et al. Desmin-Related myopathy with Mallory Body-like inclusions is caused by mutations of the Selenoprotein N gene. *Ann Neurol.* 2004;55:676–86.
- Schara U, Kress W, Bönnemann CG, Breitbach-Faller N, Korenke CG, Schreiber G, et al. The phenotype and long-term follow-up in 11 patients with juvenile Selenoprotein N1-related myopathy. *Eur J Paediatr Neurol.* 2008;12:224–30.
- von der Villar-Quiles RN, Méta y C, Gonzalez V, Donkervoort S, Bertini E, et al. The clinical, histologic, and genotypic spectrum of SEPN1-related myopathy: A case series. *Neurology.* 2020;95:e1512–27.
- Varone E, Pozzer D, Di Modica S, Chernorudskiy A, Nogara L, Baraldo M, et al. SELENON (SEPN1) protects skeletal muscle from saturated fatty acid-induced ER stress and insulin resistance. *Redox Biol Redox Biol.* 2019;24:101176.
- Filipe A, Chernorudskiy A, Arbogast S, Varone E, Villar-Quiles RN, Pozzer D, et al. Defective Endoplasmic reticulum-mitochondria contacts and bioenergetics in SEPN1-related myopathy. *Cell Death Differ.* 2021;28:123–38.
- Scoto M, Cirak S, Mein R, Feng L, Manzur AY, Robb S, et al. SEPN1-related myopathies: clinical course in a large cohort of patients. *Neurology.* 2011;76:2073–8.
- Moghadaszadeh B, Beggs AH. Selenoproteins and [internet].eir impact on human health [internet],rough diverse physiological pathways [Internet]. *Physiology.* NIH Public Access; 2006. pp. 307–15.
- Labunskyy VM, Hatfield DL, Gladyshev VN. Selenoproteins: Molecular pathways and physiological roles. *Physiol. Rev. American Physiological Society;* 2014. pp. 739–77.
- Petit N, Lescure A, Rederstorff M, Krol A, Moghadaszadeh B, Wewer UM et al. Selenoprotein N: an Endoplasmic reticulum glycoprotein with an early developmental expression pattern. *Hum Mol Genet.* 2003. pp. 1045–53.
- Chernorudskiy A, Varone E, Colombo SF, Fumagalli S, Cagnotto A, Cattaneo A, et al. Selenoprotein N is an Endoplasmic reticulum calcium sensor that links luminal calcium levels to a redox activity. *Proc Natl Acad Sci U S A.* 2020;117:21288–98.
- Pozzer D, Varone E, Chernorudskiy A, Schiarea S, Missiroli S, Giorgi C, et al. A maladaptive ER stress response triggers dysfunction in highly active muscles of mice with SELENON loss. *Redox Biol Elsevier.* 2019;20:354–66.
- Zito E, Ferreiro A. Calcium and redox liaison: A key role of Selenoprotein N in skeletal muscle. *Cells.* 2021;10:1–11.
- Arbogast S, Beuvin M, Frayssé B, Zhou H, Muntoni F, Ferreiro A. Oxidative stress in SEPN1-related myopathy: from pathophysiology to treatment. *Ann Neurol.* 2009;65:677–86.
- Hemel IMG, Sarantidou R, Gerards M. It takes two to tango: The essential role of ER-mitochondrial contact sites in mitochondrial dynamics. *Int. J. Biochem. Cell Biol. Pergamon;* 2021. p. 106101.
- Nieblas B, Pérez-Treviño P, García N. Role of mitochondria-associated Endoplasmic reticulum membranes in insulin sensitivity, energy metabolism, and contraction of skeletal muscle. *Front Mol Biosci.* 2022;9:1–17.
- Thisse C, Degraeve A, Kryukov GVG, Gladyshev VN, Obrecht-Pflumio S, Krol A, et al. Spatial and Temporal expression patterns of Selenoprotein genes during embryogenesis in zebrafish. *Gene Expr Patterns.* 2003;3:525–32.
- Wagner DE, Weinreb C, Collins ZM, Briggs JA, Megason SG, Klein AM. Single-cell mapping of gene expression landscapes and lineage in the zebrafish embryo. *Science.* 2018;360:981–7.
- Castets P, Maugeenre S, Gartioux C, Rederstorff M, Krol A, Lescure A, et al. Selenoprotein N is dynamically expressed during mouse development and detected early in muscle precursors. *BMC Dev Biol.* 2009;9:46.
- Deniziak M, Thisse C, Rederstorff M, Hindelang C, Thisse B, Lescure A. Loss of Selenoprotein N function causes disruption of muscle architecture in the zebrafish embryo. *Exp Cell Res.* 2007;313:156–67.

27. Moghadaszadeh B, Rider BE, Lawlor MW, Childers MK, Grange RW, Gupta K, et al. Selenoprotein N deficiency in mice is associated with abnormal lung development. *FASEB J*. 2013;27:1585–99.
28. Rederstorff M, Castets P, Arbogast S, Lainé J, Vassilopoulos S, Beuvin M, et al. Increased muscle stress-sensitivity induced by Selenoprotein N inactivation in mouse: A mammalian model for SEPNI-related myopathy. *PLoS One*. 2011;6:e23094.
29. Juryneć MJ, Xia R, Mackrill JJ, Gunther D, Crawford T, Flanigan KM, et al. Selenoprotein N is required for Ryanodine receptor calcium release channel activity in human and zebrafish muscle. *Natl Acad Sci*. 2008;105:12485–90.
30. Peterson SM, Freeman JL. RNA isolation from embryonic zebrafish and cDNA synthesis for gene expression analysis. *J Vis Exp*. 2009;30.
31. Link V, Shevchenko A, Heisenberg CP. Proteomics of early zebrafish embryos. *BMC Dev Biol*. 2006;6:1–9.
32. Langfelder P, Horvath S. WGCNA: an R package for weighted correlation network analysis. *BMC Bioinformatics*. 2008;9.
33. Yu G, Wang LG, Han Y, He QY. ClusterProfiler. An R package for comparing biological themes among gene clusters. *Omi J Integr Biol*. 2012;16:284–7.
34. Shahini A, Vydiyam K, Choudhury D, Rajabian N, Nguyen T, Lei P, et al. Efficient and high yield isolation of myoblasts from skeletal muscle. *Stem Cell Res Elsevier*. 2018;30:122–9.
35. Waterhouse A, Bertoni M, Bienert S, Studer G, Tauriello G, Gumienny R, et al. SWISS-MODEL: homology modelling of protein structures and complexes. *Nucleic Acids Res Oxf Acad*. 2018;46:W296–303.
36. Guex N, Peitsch MC, Schwede T. Automated comparative protein structure modeling with SWISS-MODEL and Swiss-PdbViewer: A historical perspective. Volume 30. *Electrophoresis*: John Wiley & Sons, Ltd; 2009. pp. 5162–73.
37. Smith LL, Beggs AH, Gupta VA. Analysis of skeletal muscle defects in larval zebrafish by birefringence and touch-evoked escape response assays. *J Vis Exp*; 2013.
38. Saint-Amant L, Drapeau P. Time course of the development of motor behaviors in the zebrafish embryo. *J Neurobiol*. 1998;37:622–32.
39. Drapeau P, Saint-Amant L, Buss RR, Chong M, McDearmid JR, Brustein E. Development of the locomotor network in zebrafish. *Prog Neurobiol*. 2002;68:85–111.
40. Liu DW, Westerfield M. Function of identified motoneurons and co-ordination of primary and secondary motor systems during zebra fish swimming. *J Physiol*. 1988;403:73–89.
41. Buss RR, Drapeau P. Synaptic drive to motoneurons during fictive swimming in the developing zebrafish. *J Neurophysiol Am Physiological Soc*. 2001;86:197–210.
42. Naganawa Y, Hirata H. Developmental transition of touch response from slow muscle-mediated coilings to fast muscle-mediated burst swimming in zebrafish. *Dev Biol Elsevier Inc*. 2011;355:194–204.
43. Farnsworth DR, Saunders LM, Miller AC. A single-cell transcriptome atlas for zebrafish development. *Dev Biol Elsevier Inc*. 2020;459:100–8.
44. Maiti B, Arbogast S, Allamand V, Moyle MW, Anderson CB, Richard P, et al. A mutation in the SEPNI selenocysteine redefinition element (SRE) reduces selenocysteine incorporation and leads to SEPNI-related myopathy. *Hum Mutat*. 2009;30:411–6.
45. de Oliveira AAS, Brigante TAV, Oliveira DP. Tail coiling assay in zebrafish (*Danio rerio*) embryos: Stage of development, promising positive control candidates, and selection of an appropriate organic solvent for screening of developmental neurotoxicity (DNT). *Water (Switzerland)*. 2021. p. 119.
46. Roussel Y, Gaudreau SF, Kacer ER, Sengupta M, Bui TV. Modelling spinal locomotor circuits for movements in developing zebrafish. *Elife*. 2021;10:1–35.
47. Schiaffino S, Reggiani C. Fiber types in Mammalian skeletal muscles. *Physiol Rev. American Physiological Society Bethesda, MD*; 2011;91:1447–531.
48. McDermott JC, Bonen A. Glyconeogenic and oxidative lactate utilization in skeletal muscle. *Can J Physiol Pharmacol*. 1992;70:142–9.
49. Baumann CW, Kwak D, Liu HM, Thompson LV. Age-induced oxidative stress: How does it influence skeletal muscle quantity and quality? *J Appl. Physiol. American Physiological Society*; 2016. pp. 1047–52.
50. Miyazawa H, Snaebjornsson MT, Prior N, Kafkia E, Hammarén HM, Tsuchida-Straeten N, et al. Glycolytic flux-signaling controls mouse embryo mesoderm development. *Elife*. 2022;11:83299.
51. Jackson HE, Ingham PW. Control of muscle fibre-type diversity during embryonic development: The zebrafish paradigm. *Mech. Dev. Elsevier*; 2013. pp. 447–57.
52. Cimini BA, Chandrasekaran SN, Kost-Alimova M, Miller L, Goodale A, Fritchman B, et al. Optimizing the cell painting assay for image-based profiling. *Nat Protoc*. 2023;18:1981–2013.

Publisher's note

Springer Nature remains neutral with regard to jurisdictional claims in published maps and institutional affiliations.